Regularities of fracture pattern formation in alumina ceramics subjected to dynamic indentation

E. Tolmacheva (Lyapunova)
Institute of Natural Sciences and Mathematics, Ural Federal University, Yekaterinburg, Russia
Institute of metal physics, Yekaterinburg, Russia
lyapunova@icmm.ru

M. Davydova, V. Chudinov, S. Uvarov, O. Naimark
Institute of Continuous Media Mechanics, Perm, Russia

D. Zaytsev, P. Panfilov
Institute of Natural Sciences and Mathematics, Ural Federal University, Yekaterinburg, Russia

ABSTRACT. In this paper the process of dynamic indentation, causing deformation and fracture of alumina ceramics, is investigated. The dynamic indentation experiments were carried out on the original setup based on the split Hopkinson bar technique. The regularities of structure evolution caused by indenter penetration are studied using the computer tomography data of the samples subjected to different loads. The investigation revealed the existence of comminuted area in the vicinity of the indenter and the formation of multiple cracks in the zone lying below. It was found that the higher is the applied indentation load, the denser is the crack pattern and larger are the cracks. A similarity of such a mechanical behavior between the examined material and dentin taken as a biocomposite is discussed.

KEYWORDS. Dynamic indentation; Computer tomography; Alumina; Fracture.

Citation: Tolmacheva (Lyapunova), E., Davydova, M., Chudinov, V., Uvarov, S., Zaytsev, D., Panfilov, P., Naimark, O., Regularities of fracture pattern formation in alumina ceramics subjected to dynamic indentation, Frattura ed Integrità Strutturale, 41 (2017) 552-561.

Received: 30.03.2017
Accepted: 31.05.2017
Published: 01.07.2017

INTRODUCTION

The rate effects were found to play an important role in dynamic loading of brittle materials such as dynamic indentation, ballistic impact, high-speed material processing [1-5]. The principles of static indentation mechanics would not suffice to carry out a careful analysis of the dynamic inelastic response of materials. In the existing numerical approaches there are some inherent limitations to the description of the stresses in the comminuted region of the impact zone.

Accurate experiments on dynamic loading of ceramics can provide valuable information about the rate-dependent indentation properties of structural ceramics. However, studying the fracture pattern formed under dynamic indentation of bulk ceramic samples and estimation of the damage zone size is non-trivial, because it is hidden inside the solid. Therefore a frequently used approach is the use of alternative sample geometry (planar) or experimental schemes, which can distort the results.
In this work, we employ X-ray computer tomography to reveal the inner structure of the bulk alumina ceramic samples in the damage region. It allows us to compare the regularities of the mechanical behavior of the material with the fracture pattern caused by loading.

MATERIALS AND METHODS

Alumina ceramics was produced by plasma spraying of alumina powder with average particle size of about 50 μm (Intech, Yekaterinburg). Preparation of samples includes mechanical polishing of their surface and controlling its flatness.
The standard mechanical properties of the material were investigated on the Shimadzu AGX-50kN testing machine (Institute of natural science and mathematics, Ural Federal University, Yekaterinburg, Russia) during uniaxial compression experiments at a loading rate of 100 μm/min.
Microhardness was measured by the standard Vickers microhardness testing machine (Institute of natural science and mathematics, Ural Federal University, Yekaterinburg, Russia) with the test load of 200 g.
The static and dynamic indentation experiments were carried out with standard conical indenters commonly employed in microhardness measurement equipment (base angle of 120±12° and curvature radius 0.200±0.005 mm). The static indentation experiments at a loading rate of 50...100 μm/min were carried out on the Testometric testing machine with original holder for indenter. The dynamic indentation test was performed on the modified experimental setup based on the split Hopkinson pressure bar technique [6-10]. The static and dynamic indentation experiments were conducted in the Institute of Continuous Media Mechanics, UB of RAS, Perm, Russia.
The inner structure of samples and fracture pattern formed after dynamic indentation were studied by X-ray computer tomography (*Nikon Metrology XT H 225+160 LC*) at Perm State University, Perm, Russia. The obtained resolution of tomography images was 6.1-6.3 μm/pixel for samples 9 mm in diameter and 8.3 μm/pixel for 14 mm diameter sample. ImageJ free software package [11,12] was used for numerical analysis of tomography images.

UNIAXIAL STATIC COMPRESSION EXPERIMENT

The uniaxial static compression σ-ε curves for alumina samples are shown in Fig. 1. Material toughness and elastic modulus were found to be 710±50 MPa and 6.0±0.1 GPa, respectively. Microhardness measured by standard technique with Vickers indenter was 4.0±1.2 GPa for applied load of 200 g.

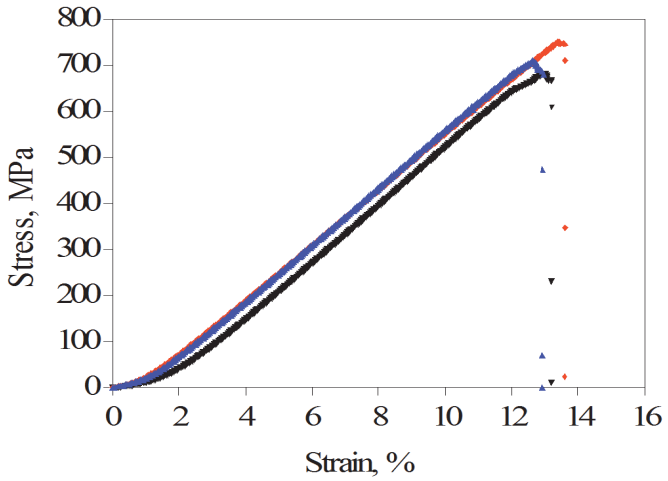

Figure 1: Uniaxial compression of alumina samples.

STATIC INDENTATION EXPERIMENT

For static indentation of ceramic samples a handmade holder was used to fix the indenter in the testing machine (Fig. 2, photo). In these experiments the indenter moved into the sample with the velocity of 50 and 100 μm/min. Static indentation force curves obtained for different loading velocities are presented at Fig. 2. It was obtained that in static experiments material does on exhibit rate sensitivity.

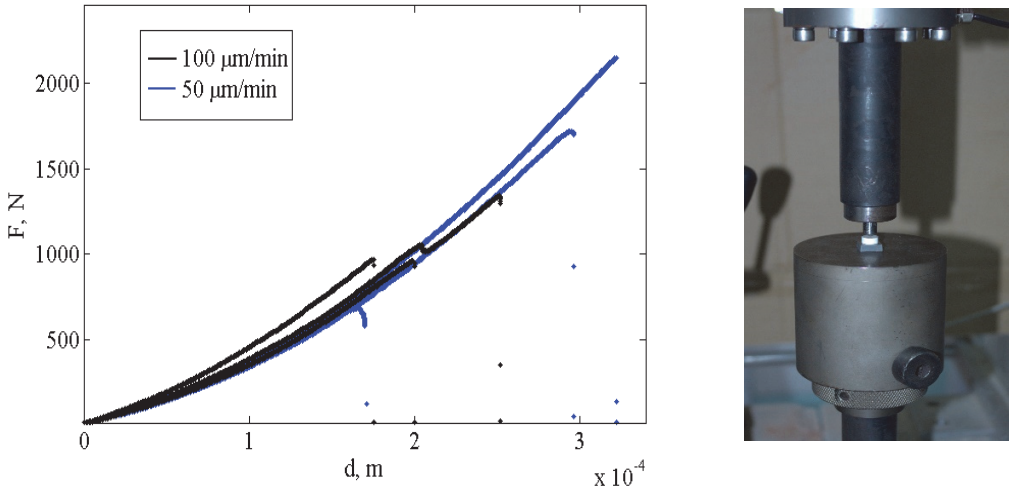

Figure 2: Static indentation of alumina samples and photo of the experiment configuration.

DYNAMIC INDENTATION EXPERIMENT

Two schemes of dynamic indentation setup were developed to achieve different amplitudes of impulse loading (Fig. 3). In both experimental schemes a sample tablet of 9 or 14 mm in diameter and 5 mm in thickness was stuck by a thin layer of glue (cyanoacrylate) onto the end surface of the hard aluminum alloy rod of 20 mm in diameter and 3 m in length. The rod with the glued sample strikes against the fixed indenter. The movement of the sample was caused by an elastic compression wave initiated in the loading rod by a collision with a stainless steel ball (7 mm in diameter, weighting 1.5 g) or a small rod of the same aluminum alloy (10 mm diameter, 70 mm length, 15.7 g mass). To produce striker acceleration in the pneumatic gas gun the stainless steel ball or aluminum alloy rod was put into the expanded polystyrene foam pallet, which has the same caliber as the pneumatic gun. Using strikers of different mass and geometry and varying the air pressure in the gas gun we could obtain loading impulses of different duration and amplitudes. For registration of the transverse compression-tension wave we used four strain gauges arranged in series along the rod surface (Fig. 3). The longitudinal displacement of the rod end surface was calculated from the gauge data by a well-established method [13]. Typical values of the sample displacement were ~100 μm and the time scale ~ 80-100 μs.

Depending on the values of the applied load, two ways of registration of the load acting on the indenter were used. For loads up to 500 N we used a piezoelectric load sensor 9217A (Kistler) with the charge meter Kistler (Fig. 3,a). Due to a difference in the designs of the load sensor and the indenter, an original stainless steel adapter was made for their coupling (denoted by 2 in Fig. 3,a and by 5 in Fig. 4). From one side the adapter provides the tight insertion and fixture of the indenter and from the other side it has M3×1 thread for fitting the load sensor (Fig. 3,a). The indenter and load sensor coupled via the adapter were fixed in the frame-like stainless steel holder 4 equipped with a limiting hollow screw 3 (Fig. 4), which protects the indenter and restricts the maximum indentation depth achieved during the experiment.

Since the load sensor used in the experiment is rated at maximum applied load of 500 N, we have used the second scheme of load registration in order to achieve higher loading amplitudes (Fig. 3,b). In this scheme, indenter 3 was screwed into additional long aluminum alloy rod 1 (Fig. 3,b) and the second line of strain gauges 2 was used to register the transmitted elastic deformation. This signal was used to calculate the value of load applied to the indenter by the sample. Such experimental scheme allowed us to obtain loading amplitudes up to 2000 N.

a)

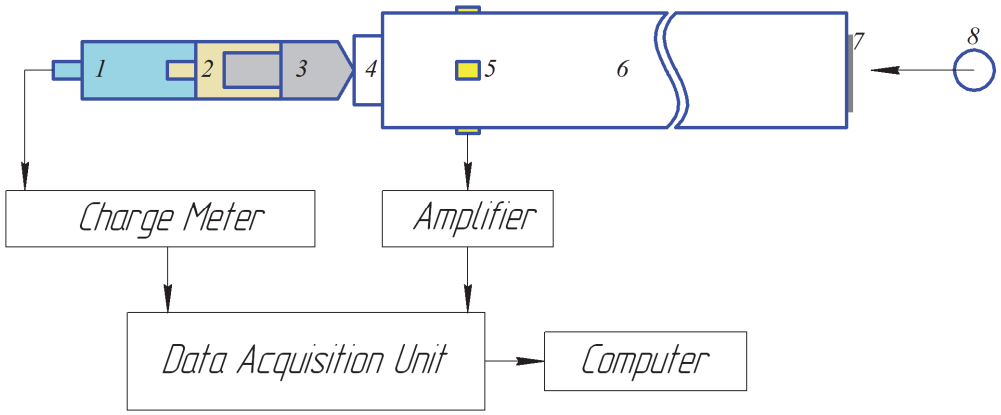

b)

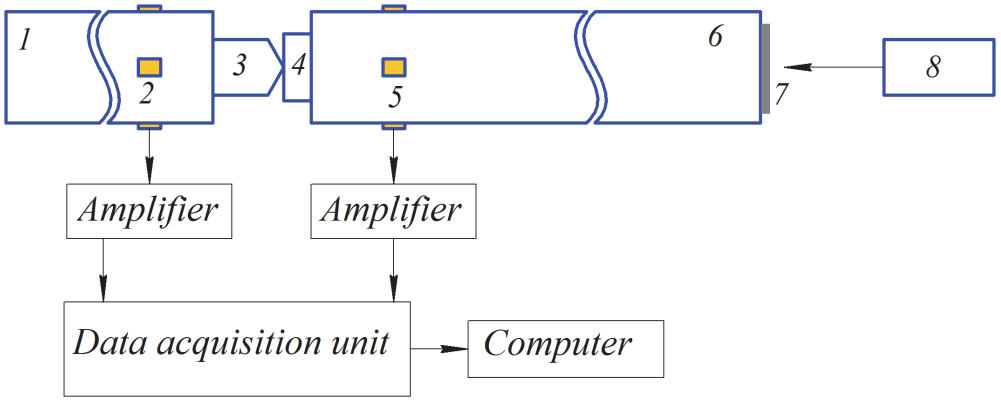

Figure 3: Dynamic indentation experiment with two types of load registration. a) For load values up to 500 N. 1 – load sensor, 2 – load sensor-indenter adapter, 3 – indenter, 4 – sample, 5 – strain gauges, 6 – loading aluminum alloy rod, 7 – shaper, 8 – stainless steel ball or small rod for initiation of the elastic compression wave in the loading rod. b) For load values up to 2000 N. 1 – aluminum alloy rod, 2 and 5 – strain gauges, 3 – indenter, 4 – sample, 6 – loading aluminum alloy rod, 7 – shaper, 8 – striker (small rod) for initiation of the elastic compression wave in the loading rod.

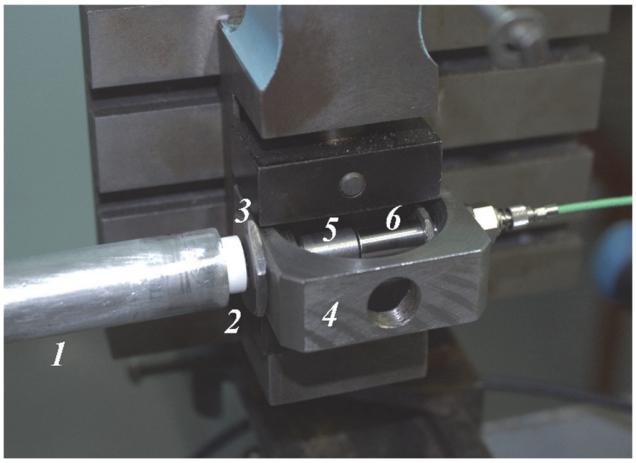

Figure 4: Mutual configuration of the loading rod, sample, load sensor and indenter-load sensor adapter in experiments with load values up to 500 N. 1 – the end part of loading rod, 2 – sample, 3 – limiting hollow screw, 4 – indenter and load sensor holder body, 5 – indenter-load sensor adapter, 6 – load sensor.

SAMPLE DISPLACEMENT CALCULATION

According to [13], the longitudinal displacement of the sample initiated by the elastic compression wave traveling through the long aluminum rod can be calculated as:

$$d = \int_0^t c_0 \left(\varepsilon_i + \varepsilon_r \right) dt \tag{1}$$

where c_0 is the sound speed in aluminum taken as 5080 m/s, ε_i and ε_r are the incident and reflected elastic impulses registered by strain gauges 5 in Fig. 3. Due to the selected experimental scheme the sample displacement is equal to the depth of indenter penetration into the sample.

Fig. 5,a illustrates typical experimental signals from the strain gauges. The elastic compression wave, initiated by the striker moves through the rod and is registered by strain gauges as the first negative peak (Fig. 5,a). After being reflected from the free end of the loading rod, the elastic wave changes into a tensile wave, which increases the displacement of the free end of the rod with glued-on sample affording thus its deeper penetration into the fixed indenter. The elastic tension wave is registered by the strain gauges as a positive peak (Fig. 5,a). Typical displacement of the sample calculated by formula (1) is shown in Fig. 5,b.

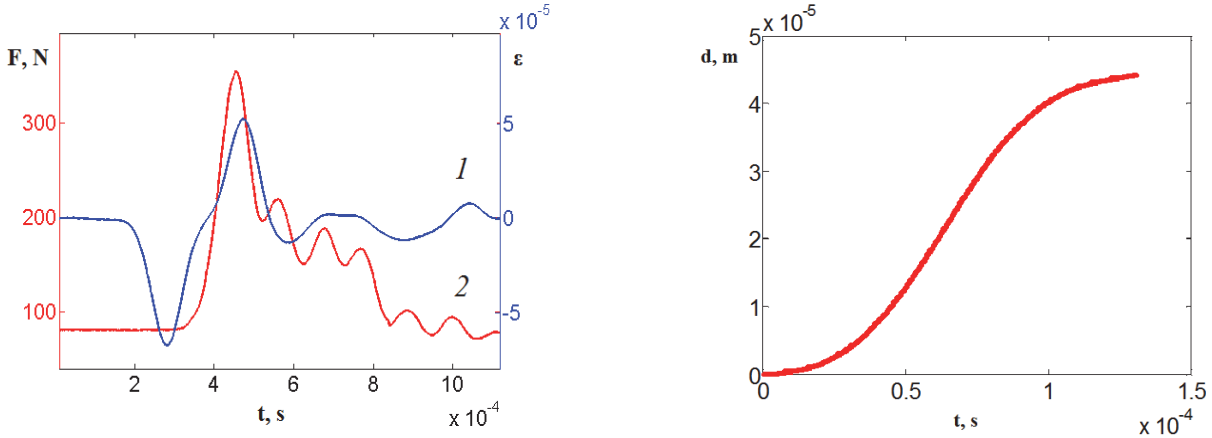

Figure 5: a) Strain gauges signal (1) and load sensor signal (2) initiated by the strike of small aluminum alloy rod accelerated to 8 m/s, b) displacement of the long rod rare surface.

LOAD CALCULATION

In the dynamic indentation experiments at a maximum load up to 500 N (first experimental scheme) the force acting on the indenter was directly registered by the piezoelectric load sensor (Fig. 5,a, curve 2). However, in the second experimental scheme we applied additional long aluminum alloy rod with another line of strain gauges in order to overcome load restrictions on the load sensor and to achieve (and detect) higher values of loading impulses. In this case, according to [13] the load acting on the indenter can be calculated as:

$$F = E\,S\,\varepsilon_t \tag{2}$$

where E and S are the elastic modulus and cross-section area of the aluminum alloy rod denoted by 1 in Fig. 3,b, ε_t is the transmitted deformation impulse registered by the strain gauges 2 in Fig. 3,b.

These data were used to construct the loading curve for dynamic indentation process in the form of the "load acting on the sample versus indenter displacement" plot.

RESULTS

Dynamic indentation loading curves.

Dynamic indentation loading curves obtained with two experimental schemes for different values of maximum load are shown in Fig. 6. For comparison, the figure also presents the initial segment of one of the static indentation curves (Fig. 2) corresponding to the loading velocity of 100 μm/min. Since in this paper we restrict our discussion only to large values of loading impulses, we show here only one curve for the first experimental scheme corresponding to a low magnitude of load (numbered as 1).

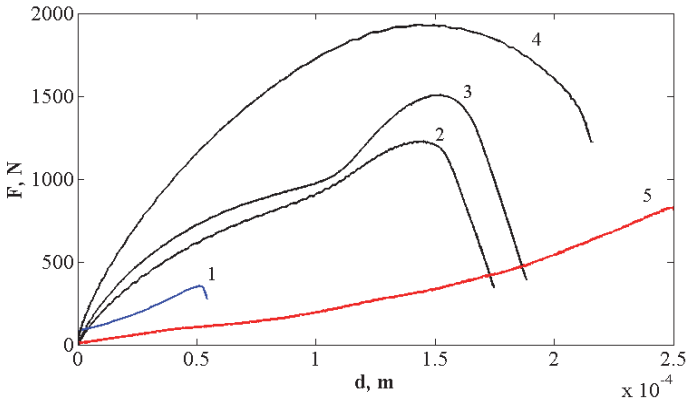

Figure 6: Dynamic indentation curves (1-4) and initial interval of static indentation curve (5).

X-ray computer tomography of deformed samples.

Four ceramic samples subjected to dynamic indentation with different maximum values of applied load were studied by X-ray computer tomography (CT). For each sample a stack of raw CT images (about 720-760 pictures) was analyzed using the ImageJ free software package [11, 12]. The internal porosity of the material as well as its fracture pattern (pores and microcracks) in the vicinity of the indenter was visualized by the thresholding technique built in the software. Typical examples of such CT images with superimposed pores/microcracks objects shown in red are presented in Figs. 7 and 9.

First, we measured the cavity radius *r* for different samples and plotted it versus the loading amplitude. As a result, we obtained a linear relationship (Fig. 7). Moreover, as expected, the crack pattern becomes more pronounced with increasing applied load (Fig. 7, upper images).

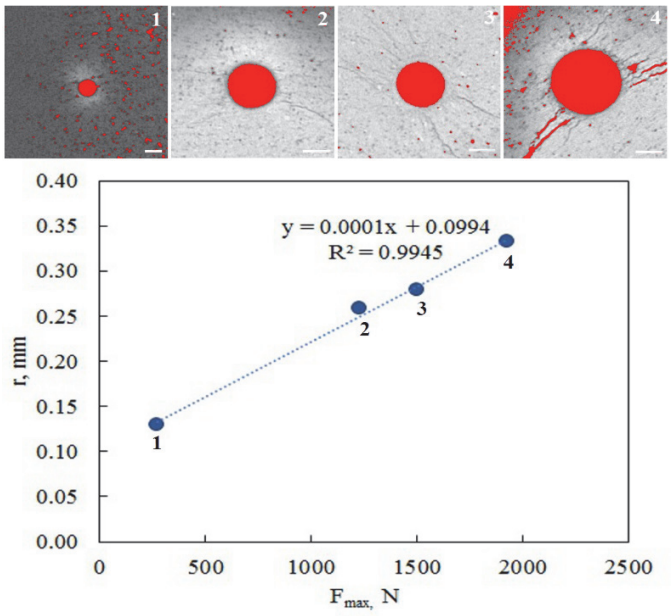

Figure 7: Radius of indentation cavity as a function of the maximum loading force. Pictures above the graph are the CT images of the corresponding cavities. Numbering of images corresponds to the numbers of dynamic indentation curves showed in Fig. 6. Scale bar size is 254 μm.

The investigation of CT images of deeper slices revealed the presence of comminuted area in the vicinity of the indenter, which can be distinguished by the local absence of pores and higher brightness corresponding to higher local density of the material. Fig. 8 presents 3D image of the inner porous structure obtained for sample no. 4 of Fig. 6 using the ImageJ visualization software package. For easy reading of the graph the forepart of the sample is veiled and the sample is rotated in such a way that the indentation direction coincides with the blue arrow (Fig. 8). We determined the depth of this comminuted area *H* for different values of the applied load, which was also found to be a linear dependence (Fig. 9). However, the width of the comminuted area *W*, calculated in plane perpendicular to the indenter penetration direction, changes non-monotonically from the surface to the deeper layers (Fig. 10). The initial interval of linearly increasing W corresponds to the indenter conical shape, whereas the following points correspond to the comminuted area in the vicinity of the indenter tip. Decay of width of comminuted area is associated with vanishing of the comminuted zone deep within the material.

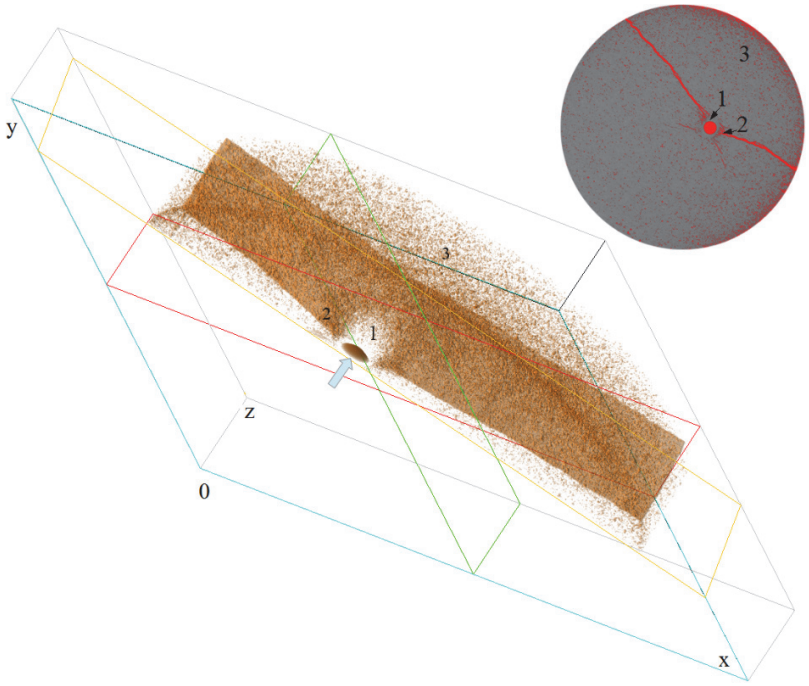

Figure 8: 3D image of inner structure of the sample no. 4 of Fig. 6. Blue arrow indicates the direction of indentation and the bottom of the cavity. 1- comminuted area, 2 – cracked area, 3 - undisturbed area. Inset: xy projection of the slice. The forepart of the sample as well as surrounding non-deformed material is veiled for easy reading of the graph.

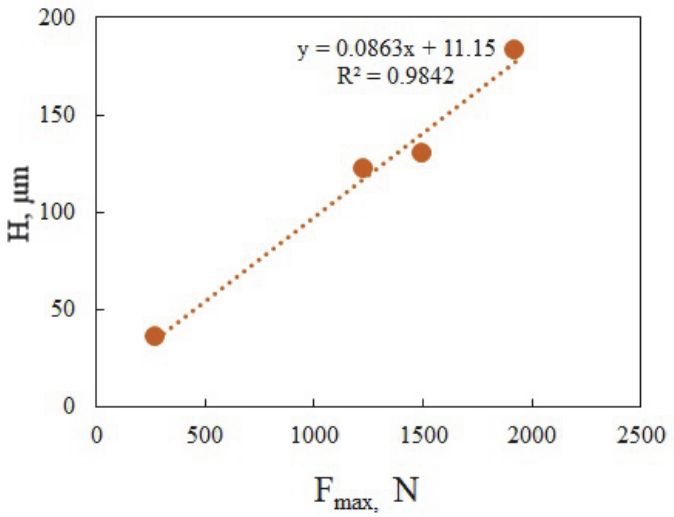

Figure 9: Depth of compressed area as a function of the maximum applied load.

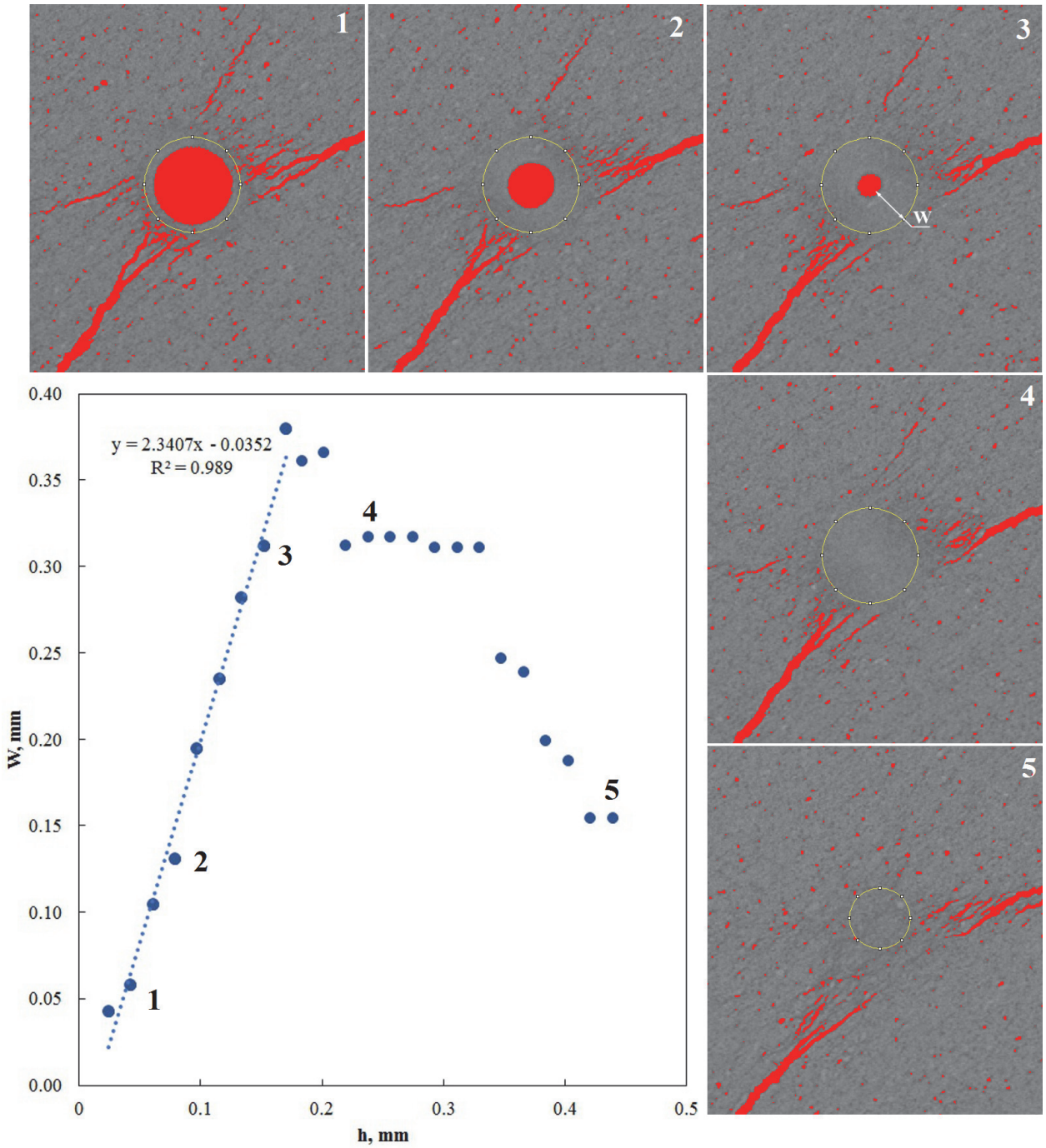

Figure 10: The width of comminuted area in the vicinity of the indenter tip at different depths of its penetration in the sample. The 3rd tomography image illustrates the way of determining the width W.

It is important that cracks formation begins not at the indenter hole, as might be expected, but at the comminuted area (Figs. 8 and 10). The ImageJ software allowed us to calculate the volumetric porosity in the comminuted area, cracked area and in region far from the process zone, which can be considered as an undisturbed area (Fig. 11). There are no points corresponding to the first amplitude of the applied load (for the sample numbered 1 in Figs. 7 and 9), because there is no cracked area for such low magnitude of the applied load. It can be seen from Fig. 11, that the comminuted area porosity is about 3 % and is practically the same for all values of the applied loads, whereas the porosity in the cracked region is an order of magnitude higher and increases with increase of the applied load from ~34 % for ~1200 N to ~45 % for ~1900 N. Porosity in the undistributed region varies between 10 and 14 % and according to rough estimation it can be considered as the initial porosity of the material.

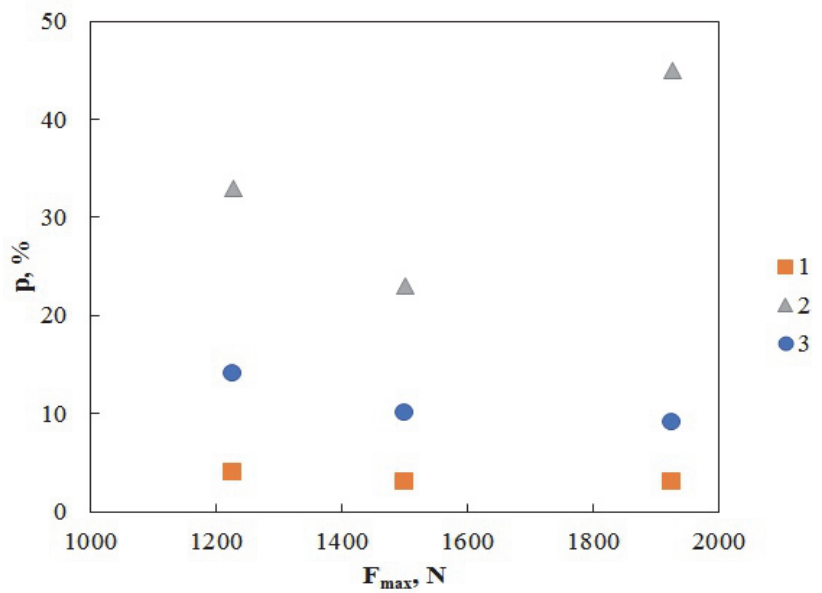

Figure 11: Porosity in different parts of the samples deformed at different maximum loads. 1 – comminuted area, 2 – cracked area, 3 – undisturbed area of the sample.

CONCLUSIONS

In this paper we discussed the results of experiments on dynamic indentation of aluminum ceramic samples, which were performed on the original setup based on the split Hopkinson bar technique. The regularities of structure evolution caused by indenter penetration were studied using the computer tomography data on samples subjected to different loads. The analysis of CT data made with the use of the ImageJ free software package revealed the existence of dense area of pressurized material (comminuted area) in the vicinity of the indenter and the formation of multiple cracks in the underlying area. It was found that the higher is the magnitude of the applied indentation load, the bigger is the diameter and height of the comminuted area. Furthermore, with the growth of the load the crack pattern becomes denser and the size of the cracks around the comminuted area increases. The porosity of the comminuted area was found to be practically the same for all values of the applied loads, whereas the porosity in the cracked region is an order of magnitude higher and continues to grow with increasing magnitude of the applied load. Porosity of the undisturbed region of the material was 4 - 5 times higher than in the comminuted area, which makes different areas with different porosity values well-distinguishable.

It is important that crack formation begins not at the indenter hole as might be expected, but at the comminuted area lying below. This circumstance can be explained by the indenter spherical tip shape. Indeed, the shape of the indenter is known to have considerable influence on the deformation (and fracture) process and the measured hardness as well. A sharp indenter produces a nominally constant plastic strain, while a spherical tip generates an increasingly growing contact stress with increase of the depth of penetration. This allows one to investigate the transition from the elastic to plastic response and to determine the contact stress-strain property of materials [14].

The obtained fracture behavior of alumina ceramics, namely, the existence of the comminuted area, which gives rise to numerous cracks, has much in common with the fracture behavior of such natural composite as dentin and enamel [15, 16]. The regularities of dynamic indentation of such biocomposite will be the subject of our future investigations.

ACKNOWLEDGMENT

The experimental study of alumina samples was supported by the Russian Science Foundation grant No. 15-19-10007.

REFERENCES

[1] Subhash, G., Maiti, S., Geubelle, P.H., Ghosh, D., Recent advances in dynamic indentation fracture, impact damage and fragmentation of ceramics. Journal of American ceramic society, 91 (2008) 2777-2791.

[2] Ghosh, D., Subhash, G., Bourne, G.R., Inelastic deformation under indentation and scratch loads in ZrB2-SiC composite. Journal of European ceramic society, 9 (2009) 3053-4061.

[3] Ghosh, D., Subhash, G., Sudatshan, T.S., Radhakrishnan, R., Gao, X.-L., Dynamic indentation response of fine-grained boron carbide. Journal of American ceramic society, 90(6) (2007) 1850-1857.

[4] LaSalvia, J.C., McCauley, J.W., Inelastic deformation mechanisms and damage in structural ceramics subjected to high velocity impact. International journal of applied ceramic technology, 7(5) (2010) 595-605.

[5] Klecka, M.A., Subhash, G., Rate-dependent indentation of structural ceramics. Journal of American society, 93(8) (2010) 2377-2383.

[6] Al-Mousawi, M.M., Reid, S.R., Deans, W.F., The use of the split Hopkinson pressure bar techniques in high strain rate materials testing. Proceedings of the institution of mechanical engineers, 211C (1997) 273-292.

[7] Bragov, A.M., Lomunov, A.K., Methodological aspects of studying dynamic material properties using the Kolsky method. International journal of impact engineering, 16 (1995) 321–330.

[8] Bragov, A.M., Demenko, P.V., Lomunov, A.K., Sergeichev, I.V., Kruszka, L., Investigation of behaviour of materials of different physical nature using the Kolsky method and its modifications. New experimental methods in material dynamics and impact, trends in mechanics of materials, eds. Nowacki W.K., Klepaczko J.R., Warsaw, (2001) 337–348.

[9] Sokovikov, M., Chudinov, V., Bilalov, D., Oborin, V., Uvarov, S., Plekhov, O., Naimark, O., Study of plastic strain localization mechanisms caused by nonequilibrium transitions in mesodefect ensembles under high-speed loading. AIP Conference Proceedings, 1683 (2015) 020218.

[10] Bilalov, D.A., Sokovikov, M.A., Chudinov, V.A., Oborin, V.A., Bayandin, Yu.V., Terekhina, A.I., Naimark, O.B. Studying plastic shear localization in aluminum alloys under dynamic loading. Journal of applied mechanics and technical physics, 57(7) (2016) 1217-1225.

[11] Abramoff, M.D., Magalhaes, P.J., Ram, S.J., Image processing with ImageJ. Biophotonics international, 11(7) (2004) 36–42.

[12] Schneider, C.A., Rasband, W.S., Eliceiri, K.W., NIH image to ImageJ: 25 years of image analysis, Nature methods. 9(7) (2012) 671.

[13] Zukas, J.A., Impact dynamic, Wiley, (1982) 452.

[14] He, L.H., Swain, M.V., Nanoindentation derived stress-strain properties of dental materials, Dental materials, 23 (2007) 814-821.

[15] Xu, H.H.K., Smith, D.T., Jahanmir, S., Romberg, E., Kelly, J.R., Thompson, V.P., Rekow, E.D., Indentation damage and mechanical properties of human enamel and dentin, Journal of dental research, 77 (1998) 472-480.

[16] Zhang, Y.-R., Du, W., Zhou, X.-D., Yu, H.-Y., Review of research on the mechanical properties of human tooth, International journal of oral science, 6 (2014) 61-69.